Pergamon

Int. J. Solids Structures Vol. 34, No. 10, pp. 1169–1182, 1997

0020-7683/97 $17.00 + .00

PII: S0020-7683(96)00110-2

CREEP DAMAGE MODELING BASED ON ULTRASONIC VELOCITIES IN COPPER

TOMOHIRO MORISHITA
Akashi College of Technology, Akashi, Hyogo 674, Japan

and

MASAHIKO HIRAO
Faculty of Engineering Science, Osaka University, Toyonaka, Osaka 560, Japan

(*Received* 29 *November* 1995; *in revised form* 17 *June* 1996)

Abstract—We measured the ultrasonic velocities and the porosity for pure copper samples subjected to the intergranular creep process. The ultrasonic velocities decreased and their anisotropy developed as the creep advanced. We study a double composite model implied by photomicrographic observations and calculated the transversely isotropic effective stiffness. In this model, spherical voids are uniformly distributed within oblate ellipsoidal volume elements. These ellipsoids are randomly embedded in an isotropic copper matrix with an axisymmetrical distribution of the minor axes around the stress direction. Incorporation of the unperturbed velocities, the porosity, and the ellipsoid aspect ratio into the modeling calculation provides the basis features of the damage morphology: the void volume fraction (in the ellipsoids) and the lowest-order expansion coefficients of the orientation distribution function (ODF). Comparison between the calculated and measured velocities was quite satisfactory, showing the validity of this micromechanical modeling.

1. INTRODUCTION

For structural materials used in a high temperature environment, creep is the most fundamental and important fracture process. Nondestructive sensing techniques have long been desired for the in-service assessment of the remaining life. Ultrasonic methods have a unique potential of detecting the internal damage state, while many others (X-ray, replication, hardness, and magnetic properties) merely inspect the surface or near-surface region of metal parts.

Ultrasonics have been studied for estimating the creep damage (Willems *et al.*, 1987; Willems, 1987; Ledbetter *et al.*, 1987; Birring *et al.*, 1989; Hirao *et al.*, 1990). As the creep proceeds, the propagation velocities of elastic waves decrease and the attenuation coefficients increase. A number of metallurgical attributes may affect the ultrasonic propagation: (i) the generation of creep voids (or cavities), (ii) the precipitation of the second phase particles such as carbides and intermetallic compounds, (iii) the texture modification by the recrystallization and the plastic deformation, and (iv) the dislocation restructuring. The creep voids and the precipitation particles introduce obstacles for the ultrasonic propagation, although their sizes are much smaller than the wavelengths.

The present study is focused on the void-velocity relationship to find what relevant information can be deduced from ultrasonic velocity measurements. The voids exert a dominant influence to the material deterioration by lowering the strength and increasing the brittleness. In the case of the intergranular creep process, which occurs at a relatively high temperature and low stress, the damage evolves accompanying the nucleation and growth of voids on the grain boundaries. Subsequent coalescence leads to microcracking and eventually macroscopic cracks occur. During this process, the mass density and the overall elastic constants are changed, which induces a monotonous decrease of the ultrasonic velocities along with their anisotropy, where the velocity depends on the propagation and polarization directions. Ledbetter *et al.* (1987) and Hirao *et al.* (1990) attempted to explain

the dependence of the ultrasonic velocities on the creep voids by regarding the voids in polycrystalline copper as oblate ellipsoids. The comparison of their modeling study and the velocity measurements showed that the velocity anisotropy was produced by the void shape and the orientation. However, the quantitative dependence was still inconclusive. In this paper, we intend to establish a damage model that explains the velocity evolution, including the anisotropy, during the creep life. For this, we measure the density and the ultrasonic velocities by interrupting the creep loading. We consider a double composite model as indicated by the photomicrographs. The spherical voids are confined to within the oblate ellipsoidal volume elements, whose minor axes may vary around the stress direction. This model allows us to determine the volume fraction of the voids (in the ellipsoids) and the orientation distribution coefficients (ODC) that give the agreement between the measured and calculated velocities. The ODCs demonstrate the progressive alignment of the ellipsoid minor axes along the stress direction and the creep voids grow primarily within the ellipsoids.

For simplicity, we assume that the ultrasonic velocities are affected only by the creep voids. To avoid precipitation, pure copper is used. To suppress the change of the metallurgical structure, a stabilization annealing is provided prior to the creep tests. The test conditions are chosen for intergranular creep fracture to take place. There should be no plastic deformation, because the rupture occurred in a brittle manner, leaving little elongation of the specimens.

2. EXPERIMENTS

2.1. *Creep test*

The test material is a commercial tough pitch copper of 99.95 mass pct purity. The creep specimens were machined from a rolled plate of 20 mm thick. The plate was annealed at 800°C, which was higher than the creep temperature, for 3 hours before machining. They were further annealed at 550°C for 20 hours before the creep tests. Specimen geometry and sample coordinate system $0-x_1x_2x_3$ are shown in Fig. 1. The x_1 direction lies along the thickness direction of the original plate and the x_2 along the rolling direction. Eight specimens were crept to failure in air, four at 500°C and the other four at 550°C to know the time to rupture. The nominal stress was 6.0 MPa at the minimum cross section. The temperature was held within 2°C; its spatial variation along the specimen gauge length was less than 2°C. The test conditions and the rupture times are listed in Table 1. The average rupture time, t_r, was 597.8 hours at 500°C and 270.8 hours at 550°C. The elongation of the ruptured specimens was negligible despite the fairly high ductility at the room temperature. Brittle fracture occurred without any visible precursors. The location was within 10 mm of the minimum cross section.

We made interrupt tests in the same creep conditions as the rupture tests to obtain coupons for the density and velocity measurements. Eleven interrupting times were chosen

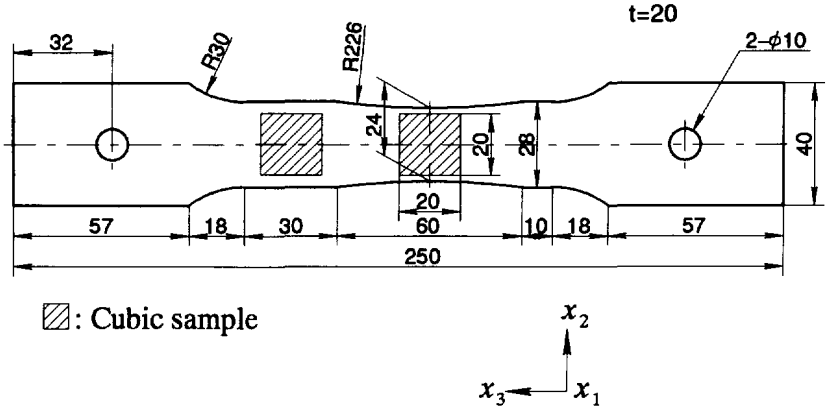

Fig. 1. Specimen geometry and sample coordinate system $0-x_1x_2x_3$.

Table 1. Creep test conditions and rupture time

Stress	(MPa)	6.0	
Temperature	(°C)	500	550
Rupture time	(hr)	618.9	279.2
		573.1	264.2
		580.5	267.3
		618.6	272.6
	t_r	597.8	270.8
Time of interrupt test	t/t_r	0.1 0.2 0.3 0.4 0.5 0.6 0.7 0.75 0.8 0.85 0.9	

relative to t_r as shown in the bottom row of Table 1. Shallow notches were introduced to obtain two cube samples, 20 mm on each side, of different damage states (Fig. 1). They underwent slightly different stresses with the equal thermal history. Because the stress concentration factor at the notch bottom was estimated as 1.04 from a finite element computation, we ignored the damage inhomogeneity around the notches. Here we refer to them as the interrupt samples. For a comparison purpose, we prepared six reference samples of the same dimensions from a specimen after the heat treatment.

Figure 2 is a typical photomicrograph. The grain shape is nearly equiaxial and the grain size is approximately 0.1 mm. Voids are not randomly positioned. They tend to gather preferentially on the grain boundaries perpendicular to the x_3 direction. The void diameter is approximately 10 μm at this stage of creep.

2.2. *Porosity*

The porosity c is defined by the decreasing rate of density,

$$c = 1 - \frac{\rho_*}{\rho_0}, \tag{1}$$

where "0" and "*" indicate the reference (uncrept) and interrupt samples, respectively. We determined c from the weight measurements as Ratcliffe (1965) did:

$$c = 1 - \frac{W_*^a(W_0^a - W_0^w)}{W_0^a(W_*^a - W_*^w)}, \tag{2}$$

where "a" and "w" indicate the weights in air and in water. The measuring error was estimated to be less than $\pm 10^{-4}$. This measurement of c is independent of the sample volume and the fluid density.

Figure 3 shows the change of c with creep time. For the samples from the notches, c increased at the accelerating rates. The value of c at rupture depends on the creep condition. The samples from the smooth positions displayed a slower increase because of the slightly lower stress. The creep tests were duplicated at 550°C for $t/t_r = 0.8$, 0.85, and 0.9. The difference for nominally the same creep condition arises probably from the metallurgical inhomogeneity, which causes a variation in the rupture time or the damage accumulation rate in the individual specimens.

2.3. *Ultrasonic velocities*

We measured the velocities of nine plane waves propagating and polarized in the principal directions using a sing-around technique for the broad-band echoes generated and received by 7.5 mm square piezoelectric transducers. The center frequency was 10 MHz for longitudinal waves and 5 MHz for shear waves. The velocities were given by dividing twice the thickness by the transit time difference between first and second echoes. The accuracy was $\pm 1.3 \times 10^{-3}$ in terms of V/V^0, where V^0 denotes the average velocities over six reference samples. The reference samples showed an intrinsic orthorhombic anisotropy

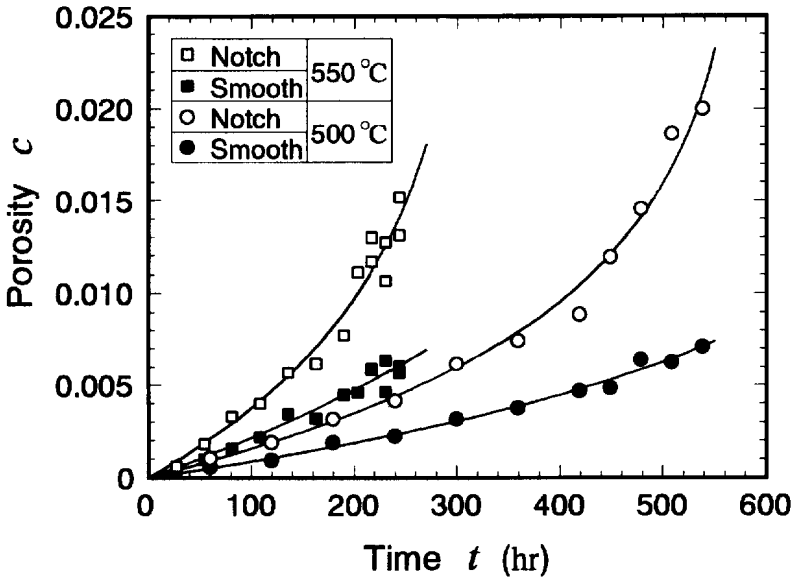

Fig. 3. Evolution of porosity c with creep time. Least-square fitting curves are $c = (1 - t/a)^b$, where $a = 324$ hr and $b = 0.0103$ for 550°C/Notch; $a = 623$ hr and $b = 0.0124$ for 550°C/Smooth; $a = 585$ hr and $b = 0.0084$ for 500°C/Notch; $a = 823$ hr and $b = 0.0068$ for 500°C/Smooth.

Table 2. Ultrasonic velocities in the reference sample

		Polarization direction		
		x_1	x_2	x_3
Propagation direction	x_1	4726	2303	2287
	x_2	2308	4723	2284
	x_3	2281	2285	4734

due to the rolling texture. In Table 2, exchanging the propagation and polarization directions leaves the shear wave velocity virtually unchanged. Maximum velocity difference is 0.23 pct for longitudinal waves and is 1.17 pct for shear waves. The creep loading creates a damage-induced anisotropy, which has the axes coincident with the original principal axes and is regarded to be superimposed upon the texture-induced anisotropy.

The oriented growth of voids makes the copper samples transversely isotropic around the stress axis. We measured nine velocities, but there are only four independent velocity variations that reflect the deterioration. The relations between the porosity c and the normalized velocities are shown in Fig. 4. V_{ij} refers to the velocity of elastic wave propagating in the x_i direction and polarized in the x_j direction. The solid lines represent the least-square fitting with polynomials. The longitudinal wave suffered from a severe damping in the final stage of creeping. The velocity V_{33}, which is most sensitive to the creep damage, was not obtainable for $c > 0.018$. The ultrasonic velocities decrease monotonously with increasing c. The normalized velocity V_{11}/V_{11}^0 equals V_{22}/V_{22}^0 within the error band and the mean values are plotted. Similar coincidence is seen between V_{12} and V_{21}, and among V_{13}, V_{23}, V_{31} and V_{32}.

3. CREEP DAMAGE MODELING

3.1. *Double composite modeling for integranular creep*

The ideal transverse isotropy of evolving velocities in Fig. 4 stimulates us to simplify the reference samples to be isotropic as far as the calculation of the normalized velocities is concerned. Averaging the ultrasonic velocities gives $\sqrt{(\lambda_0 + 2\mu_0)/\rho_0} = 4727$ m/s and $\sqrt{\mu_0/\rho_0} = 2292$ m/s from Table 2. Mass and volume measurements gave $\rho_0 = 8.89$ g/cm^3, which yields the unperturbed values of bulk modulus $K_0 = 136$ GPa and shear modulus $\mu_0 = 46.7$ GPa.

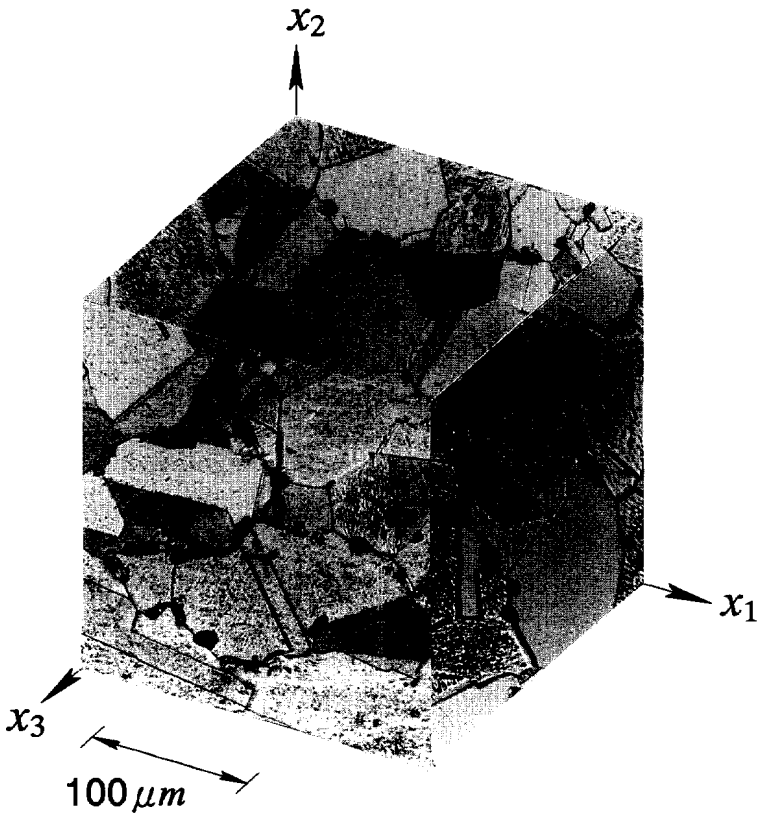

Fig. 2. Photomicrograph of creep damaged copper; notched position, $t/t_r = 0.7$, 550°C, 6.0 MPa.

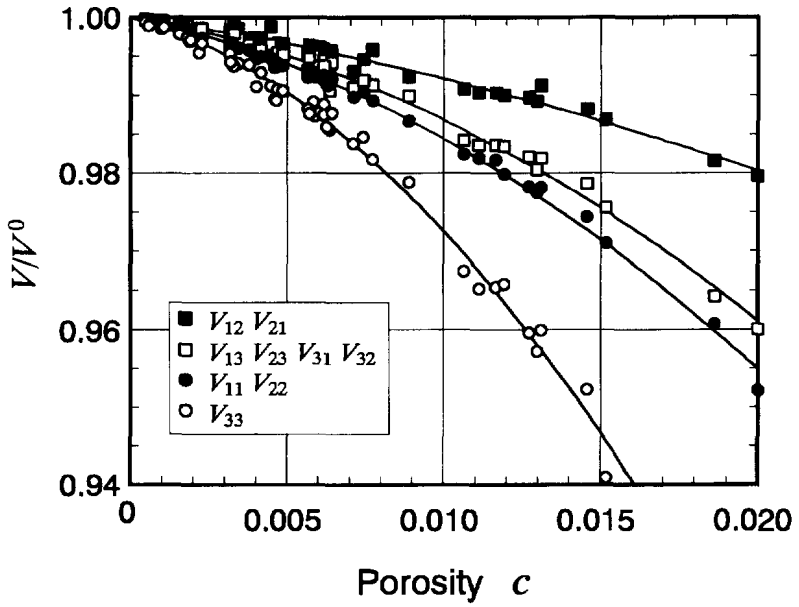

Fig. 4. Relations between porosity c and normalized ultrasonic velocities. There are only four independent variations because of the transverse isotropy. Polynomial fitting curves are, $V_{11}/V_{11}^0 = 1-0.86c-70c^2$, $V_{33}/V_{33}^0 = 1-1.1c-160c^2$, $V_{12}/V_{12}^0 = 1-0.59c-20c^2$, $V_{13}/V_{13}^0 = 1-0.68c-63c^2$.

We consider a creep-damaged copper as a two-phase composite material comprising the isotropic copper matrix and the voids. To account for the transversely-isotropic effective stiffness, we have the option of modeling either of the following three features or combination thereof: the void shape and the nonrandom distribution of their location and orientation. Ledbetter *et al.* (1987) proposed a simple model for this purpose. They supposed that oblate ellipsoidal voids distribute randomly in the matrix and their minor axes are perfectly aligned in the stress direction. Unfortunately, this model is incapable of explaining satisfactorily the dependence of the longitudinal wave velocities on the voids. This is also the case even if the polarized shear waves participated (Hirao *et al.*, 1990).

The damage morphology observed by photomicrograph motivates us to consider a composite modeling relying on the nonrandom positions of spherical voids. The basic concept is illustrated in Fig. 5 in a two-dimensional sketch. The creep voids are assumed to be dispersed uniformly in oblate ellipsoidal volume elements. The volume elements are randomly positioned in the matrix, but their minor axes (X_3) are statistically tilted in an axisymmetric way.

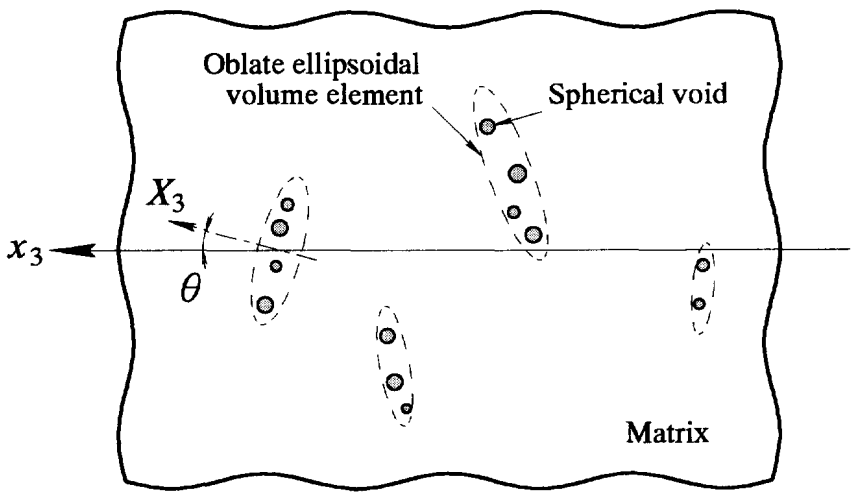

Fig. 5. Double composite modeling for integranular creep process.

The calculation procedure with this *double composite model* consists of three steps. First, the spherical voids are assumed to be distributed uniformly in the copper matrix. We calculate the effective stiffness and the overall density for the porous material. Second, the oblate ellipsoidal inclusions, whose density and stiffness are known from the previous step, are distributed randomly in the copper matrix with the minor axes parallel to the stress direction and the effective stiffness is obtained. Finally, the oblate ellipsoids are inclined by an angle θ and then the resultant stiffness is averaged for the weighted distribution of θ. To represent the orientation distribution of the ellipsoids, we introduce the orientation distribution function (ODF) developed by Roe (1965). To date, the ODF has been used to study the aggregate elastic constants in textured polycrystalline metals (Sayers, 1982; Hirao *et al.*, 1987), rocks containing microcracks (Sayers, 1990), and short-fiber composites (Sayers, 1992; Dunn and Ledbetter, 1996). Their successes encourage us to apply the ODF to creep damage modeling. The composite model having such a hierarchical structure has been used for studying the elastic stiffness of SiC/Al-alloy composite by Ledbetter *et al.* (1984). The present treatment draws much on the previous work by many researchers, especially of Sayers (1992).

For the first step, we calculate the effective moduli using the formula derived by Weng (1984), which is based on Mori-Tanaka's (1973) "average stress' and is applicable to a dense concentration of inclusions. Ledbetter and Datta (1986) gave an alternative expression using a scattered-plane-wave ensemble average model. These two approaches give the same values of effective moduli for the random distribution of voids up to extremely high concentration. We use Weng's formula and substitute the isotropic, homogeneous elastic constants for the matrix and zero stiffness for spherical voids. This yields the explicit expressions for the effective bulk modulus K_2 and the effective shear modulus μ_2:

$$\frac{K_2}{K_0} = 1 + \frac{c_1}{\dfrac{3(1-c_1)K_0}{3K_0+4\mu_0} - 1}, \tag{3}$$

$$\frac{\mu_2}{\mu_0} = 1 + \frac{c_1}{\dfrac{6}{5}\dfrac{(1-c_1)(K_0+2\mu_0)}{3K_0+4\mu_0} - 1}, \tag{4}$$

where c_1 is the volume fraction of spherical voids and "0" stands for the matrix. The density of the composite, ρ_2, is

$$\rho_2 = (1-c_1)\rho_0. \tag{5}$$

In the second step, the shape of the oblate ellipsoids is represented by an aspect ratio $\alpha(<1)$ defined by $\alpha = r_3/r_1$, where $r_1(=r_2)$ and r_3 are the radii along the major and minor axes of oblate ellipsoids. Tandon and Weng (1984) and Zhao *et al.* (1989) have presented the effective engineering elastic constants for the transversely isotropic symmetry. We substitute K_2 and μ_2 into their expressions to obtain the anisotropic stiffness tensor for the perfect alignment, C^a_{ijkl}. The volume fraction of the oblate ellipsoids is denoted by c_2. We refrain from recasting their expressions. The stiffness tensor C^a_{ijkl} has five independent elastic constants. They are $C^a_{11} = C^a_{22}, C^a_{33}, C^a_{12} = C^a_{21}, C^a_{23} = C^a_{32} = C^a_{31} = C^a_{13}, C^a_{44} = C^a_{55}$, and $C^a_{66} = (C^a_{11} - C^a_{12})/2$ in the Voigt (two-index) notation; all others are zero. The density of the composite is

$$\rho_a = (1-c_2)\rho_0 + c_2\rho_2 = (1-c_1c_2)\rho_0. \tag{6}$$

Up to this point, the effective stiffness tensor C^a_{ijkl} is governed by c_1, c_2 and α provided the elastic constants of the copper matrix are known. The porosity c is determined by $c = c_1c_2$.

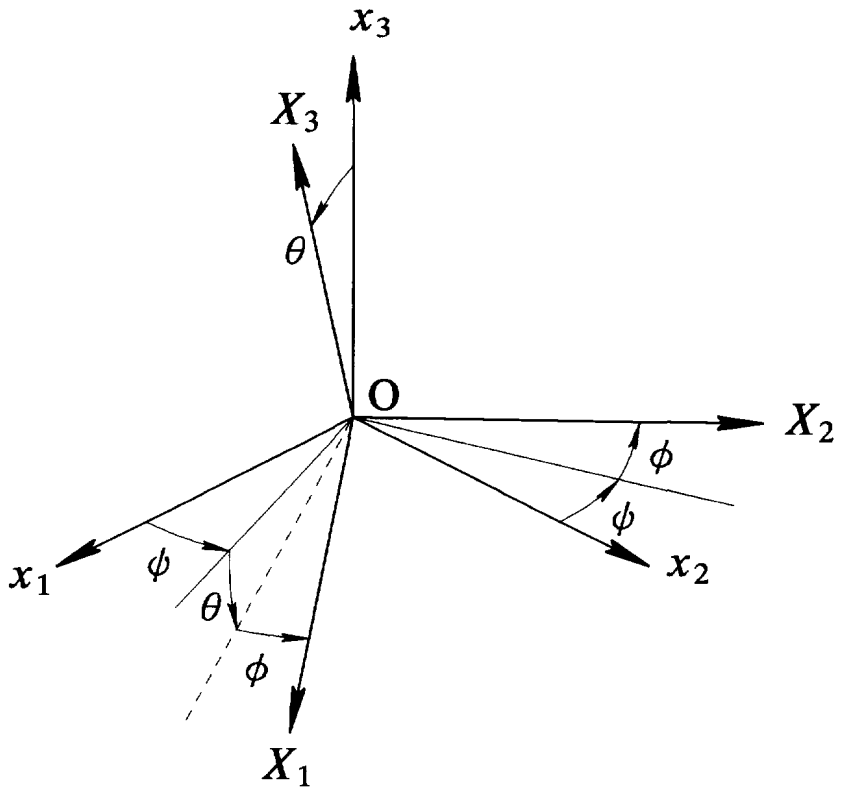

Fig. 6. Euler angles, ψ, θ, ϕ, connecting the sample coordinate system $0-x_1x_2x_3$ to the ellipsoid coordinate system $0-X_1X_2X_3$.

3.2. *Orientation distribution function*

The sample coordinates $0-x_1x_2x_3$ and the ellipsoid coordinate system $0-X_1X_2X_3$ are related to each other through the Euler angles in Fig. 6; the X_3 coordinate is taken along the minor axis of the ellipsoid. Using the ODF $w(\xi,\psi,\phi)$, where $\xi=\cos\theta$, we have the probability $w(\xi,\psi,\phi)\,\mathrm{d}\xi\,\mathrm{d}\psi\,\mathrm{d}\phi$ of finding the ellipsoidal elements whose orientations are between (ψ,θ,ϕ) and $(\psi+\mathrm{d}\psi,\theta+\mathrm{d}\theta,\phi+\mathrm{d}\phi)$. The integration of this probability density over all possible orientations should be unity;

$$\int_0^{2\pi}\int_0^{2\pi}\int_{-1}^{1} w(\xi,\psi,\phi)\,\mathrm{d}\xi\,\mathrm{d}\psi\,\mathrm{d}\phi = 1. \tag{7}$$

The ODF w is expanded in a series of generalized spherical harmonics as

$$w(\xi,\psi,\phi)=\sum_{l=0}^{\infty}\sum_{m=-l}^{l}\sum_{n=-l}^{l} W_{lmn}Z_{lmn}(\xi)\exp(-im\psi)\exp(-in\phi), \tag{8}$$

where $Z_{imn}(\xi)$ is the generalization of associated Legendre functions (Roe, 1965). The expansion coefficients W_{lmn} are called the orientation distribution coefficients (ODCs). If l, m, or n is odd, $W_{lmn}=0$. Normalization condition eqn (7) implies $W_{000}=1/(4\sqrt{2\pi^2})$.

3.3. *Average weighted by ODF*

The third step of the model calculation is the average of the stiffness tensor C^a_{ijkl} weighted by the ODF $w(\xi,\psi,\phi)$. The stiffness C^a_{ijkl} expressed with the ellipsoid coordinates is transformed to that in the sample coordinates by multiplying

$$T_{mnpqijkl}=\beta_{mi}\beta_{nj}\beta_{pk}\beta_{ql}, \tag{9}$$

where β_{mi} is the direction cosine between the X_m and x_i axes. The transformed stiffness is

then weighted by $w(\xi, \psi, \phi)$ and integrated to have the final expression, C^*_{ijkl}, for the double composite model with the partially aligned oblate ellipsoids:

$$C^*_{ijkl} = \bar{T}_{mnpqijkl} C^a_{mnpq}, \tag{10}$$

where

$$\bar{T}_{mnpqijkl} = \int_0^{2\pi} \int_0^{2\pi} \int_{-1}^{1} T_{mnpqijkl} w(\xi, \psi, \phi)\, \mathrm{d}\xi\, \mathrm{d}\psi\, \mathrm{d}\phi. \tag{11}$$

Since the elastic stiffness tensor is of the fourth rank, C^*_{ijkl} contains W_{lmn} up to $l = 4$.

The effective anisotropic stiffness C^*_{ijkl} depends only on W_{200} and W_{400} as established by incorporating the circular cross section of the ellipsoids and the transverse isotropy of the macroscopic stiffness. The explicit form of ODF w is then

$$w(\xi) = \frac{1}{8\pi^2} + \frac{1}{2\sqrt{2}}\left[\sqrt{5}(3\xi^2 - 1) W_{200} + \frac{3}{4}(35\xi^4 - 30\xi^2 + 3) W_{400}\right]. \tag{12}$$

Finally, the C^*_{ijkl} are given by

$$\begin{aligned}
C^*_{11} &= \lambda^* + 2\mu^* + \frac{8\sqrt{10}}{105}\pi^2 a_3 W_{200} + \frac{4\sqrt{2}}{35}\pi^2 a_1 W_{400},\\
C^*_{33} &= \lambda^* + 2\mu^* - \frac{16\sqrt{10}}{105}\pi^2 a_3 W_{200} + \frac{32\sqrt{2}}{105}\pi^2 a_1 W_{400},\\
C^*_{44} &= \mu^* - \frac{2\sqrt{10}}{315}\pi^2 (7a_2 + 2a_3) W_{200} - \frac{16\sqrt{2}}{105}\pi^2 a_1 W_{400},\\
C^*_{66} &= \mu^* + \frac{4\sqrt{10}}{315}\pi^2 (7a_2 + 2a_3) W_{200} + \frac{4\sqrt{2}}{105}\pi^2 a_1 W_{400},\\
C^*_{31} &= \lambda^* + \frac{4\sqrt{10}}{315}\pi^2 (7a_2 - a_3) W_{200} - \frac{16\sqrt{2}}{105}\pi^2 a_1 W_{400},\\
C^*_{12} &= \lambda^* - \frac{8\sqrt{10}}{315}\pi^2 (7a_2 - a_3) W_{200} + \frac{4\sqrt{2}}{105}\pi^2 a_1 W_{400},
\end{aligned} \tag{13}$$

where

$$\begin{aligned}
\lambda^* &= \tfrac{1}{15}(C^a_{11} + C^a_{33} + 5C^a_{12} + 8C^a_{13} - 4C^a_{44}),\\
\mu^* &= \tfrac{1}{30}(7C^a_{11} + 2C^a_{33} - 5C^a_{12} - 4C^a_{13} + 12C^a_{44}),\\
a_1 &= C^a_{11} + C^a_{33} - 2C^a_{13} - 4C^a_{44},\\
a_2 &= C^a_{11} - 3C^a_{12} + 2C^a_{13} - 2C^a_{44},\\
a_3 &= 4C^a_{11} - 3C^a_{33} - C^a_{13} - 2C^a_{44}.
\end{aligned} \tag{14}$$

The moduli λ^* and μ^* are the isotropic constants and a_i $(i = 1, 2, 3)$ are the anisotropy factors. They have been all obtained in the second step of calculation in terms of the ellipsoid aspect ratio α, the volume fractions c_1 and c_2 $(c = c_1 c_2)$, and the matrix (isotropic) elastic constants. There are then five parameters, c_1, c_2, α, W_{200}, and W_{400} that determine the C^*_{ijkl} in the double composite modeling for the creep damage. Both a_i and W_{l00} $(l = 2, 4)$ contribute to the stiffness anisotropy. The a's reflect the anisotropy strength introduced by

the arranged formation of spherical voids on the grain boundaries. The two ODCs reflect the orientation distribution of the oblate ellipsoids containing the voids inside. When the ellipsoids are randomly oriented, the ODCs vanish and there is no stiffness anisotropy, leaving only λ^* and μ^*, which are decreased by the void formation.

4. COMPARISON BETWEEN CALCULATED AND MEASURED VELOCITIES

For the elastic waves propagating and polarized in the principal directions of the transverse anisotropy, the velocities are simply obtained by the square root of the corresponding stiffness divided by the overall density; $V_{11}^* = \sqrt{C_{11}^*/\rho_*}$, $V_{33}^* = \sqrt{C_{33}^*/\rho_*}$, $V_{13}^* = \sqrt{C_{44}^*/\rho_*}$, $V_{12}^* = \sqrt{C_{66}^*/\rho_*}$, where $\rho_* = \rho_a$ of eqn (6). Both the density and the stiffness are reduced by the voids. The stiffness decreases more than the density, leading to the velocity decrease.

We compare the measured velocities with the prediction by the double composite modeling and discuss the validity for the modeling parameters. If c_1, c_2, α, W_{200}, and W_{400} were all known, it would be straightforward to calculate the velocities following the steps described. We intend to infer these five parameters from the measured velocities. We take a numerical solution by minimizing the sum of the squared errors defined by

$$E = \sum_{i=1}^{4} (u_i^m - u_i^p)^2, \tag{15}$$

by suitably choosing the parameters. The measurement and the prediction are indicated by "m" and "p" for the normalized velocities $u = V/V^0$. We employ the conjugate direction method by Powell (1964). Direct inversion approach for all five unknowns failed, since the solution depends on the initial values for the iteration calculations. Using the measured porosity $c = c_1 c_2$ and working with four unknowns (c_1, α, W_{200}, W_{400}), we obtain a too small α. Figure 7 shows the dependence of E_{min} on α for $c = 0.005$, 0.010, and 0.015. Our scheme is incapable of minimizing E at a finite α and the solution for α is unobtainable. Moreover, c_1 exceeds 1 when α is close to 1. For the sake of supplement, we then impose $\alpha = 0.1$ on the calculation. This is suggested by the average void diameter of 10 μm and the average grain size of 0.1 mm. We thus solve the three unknowns (c_1, W_{200}, W_{400}) by achieving a minimum E with four normalized velocities at each interrupted creep loading.

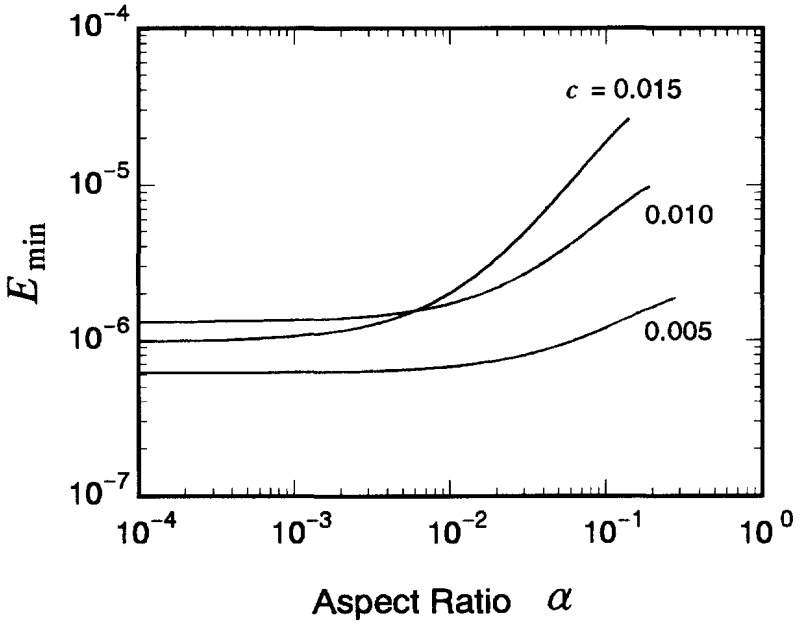

Fig. 7. Minimum error E as a function of α for three porosities.

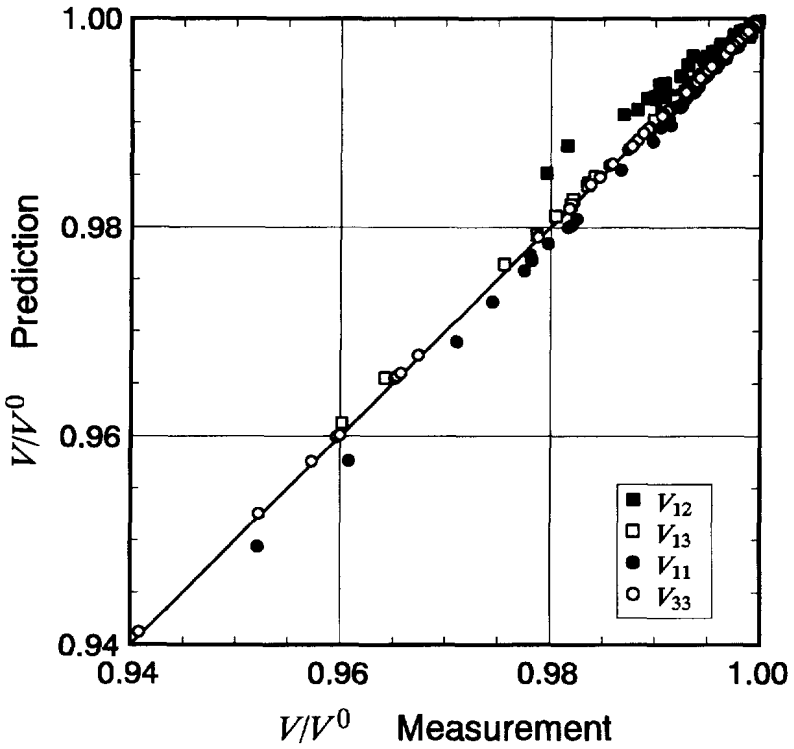

Fig. 8. Agreement between the measured and predicted velocity variations.

Figure 8 compares the measured and predicted velocities. We see a satisfactory agreement of four independent velocity evolutions throughout the creep life. The double composite model is, therefore, appropriate and is capable of explaining the void-velocity relationship for the damage estimation. Three inferred parameters are shown in Fig. 9. Iteration on eqn (15) was repeated, say, ten times until the minimum E in the order of 10^{-5} was reached. The oblate-ellipsoid volume fraction c_2 is also plotted, which is calculated from inferred c_1 with the measured porosity c. The solid lines show the calculated results based on the fitting curves in Fig. 4. The fitting curve on V_{33} is extrapolated to compensate for V_{33}, which was unavailable in the last two measurements. As the creep progresses, the two volume fractions increase. The ellipsoid elements are sparsely scattered in the matrix, but they continue to grow in volume, containing more and more voids in them. High volume fraction c_1 shows that the voids of various sizes are closely packed in the ellipsoids. The ODCs also tend to increase as a whole, though not so evident as c_1. This evolution indicates the anisotropy growth due to the preferential void formation. Figure 10 presents the ODF w obtained by substituting the inferred ODCs at $c = 0.005$ and $c = 0.015$ into eqn (12). The inverted ODF demonstrates the high concentration around $\theta = 0$, which is enhanced as the creep advances. This result is also compatible with the photomicrographic observations. Ultrasonic velocity renders only two lowest order ODCs, W_{200} and W_{400}, which is the origin of losing the fine features of the orientation distribution and is responsible for yielding unrealistic negative values of w.

When the voids start to nucleate, their sites are not many enough to make the clusters (in the oblate ellipsoids). The transverse isotropy is still in its infancy with infinitesimal ODCs. Then, the predicted ODCs for $c < 0.005$ in Fig. 8 are likely to be erroneous. This is partially caused by the behavior that the anisotropy factors a_i $(i = 1, 2, 3)$ approach zero when c_1 diminishes. The magnitude for a_3 is one-order larger than those of a_1 and a_2 over the whole creep life, which is responsible for more scattering with W_{400}. In the reversed sense, W_{400} contributes little to the transversely-isotropic stiffness tensor. Ignorance of the texture-induced anisotropy can be another error source. In the early stage, the damage-induced anisotropy is overwhelmed by the texture effect and the calculation procedure based on the hypothetical isotropic matrix fails to reduce the acceptable ODCs.

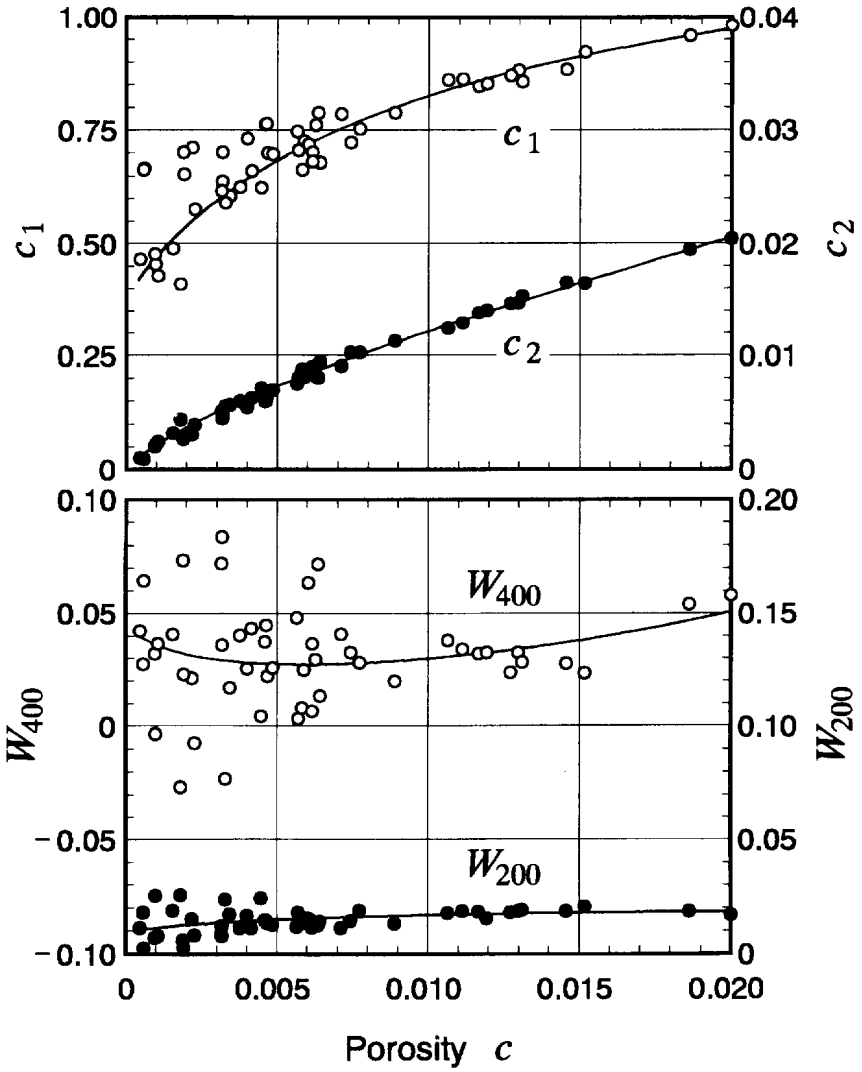

Fig. 9. Predicted volume fractions and ODCs of the crept copper. A constant aspect ratio 0.1 is assumed. The value for c_2 is given by dividing the measured c by c_1.

5. CONCLUSION

We have measured the propagation velocities of the longitudinal waves and polarized shear waves along the principal directions of the crept copper samples. Velocity measurements can detect the elastic softening and the development of the transverse isotropy in the overall stiffness, providing a bulk-average information pertinent to considering the damage morphology. We proposed the double composite model based on metallographical observations. Comparison between the predicted and the measured velocities was quite satisfactory over the whole creep life. The present model reveals that the spherical voids nucleate and grow preferentially on the grain boundaries perpendicular to the stress. The clustering region, which is modeled as oblate ellipsoids, does not expand much during the creep life, but the void concentration increases to a high level. The ellipsoid minor axes are tilted by small angles around the stress axis from the early stage. As the damage accumulates, the orientation is further concentrated along the stress axis. The double composite model is then a useful micromechanical model for discussing the macroscopic effects of the creep voids causing the grain boundary deterioration. Separation of the texture-induced anisotropy remains for further study.

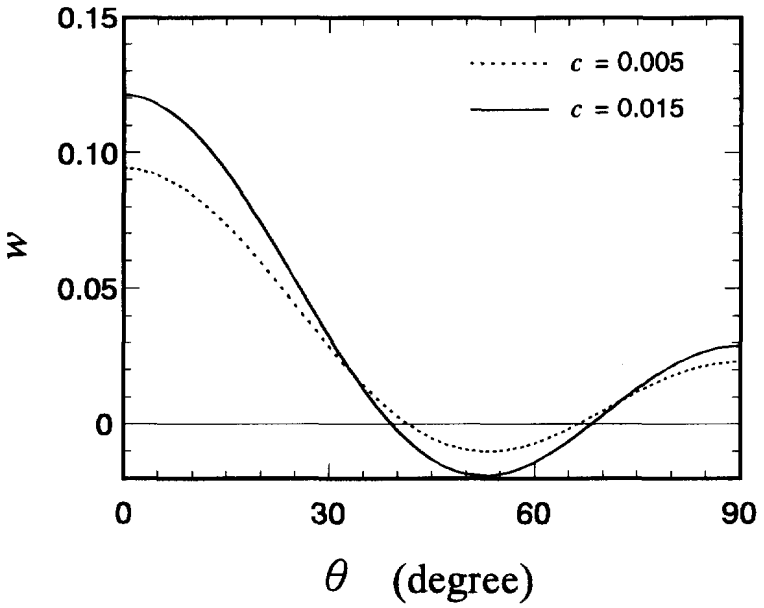

Fig. 10. Orientation distribution of the ellipsoid normals at $c = 0.005$ and $c = 0.015$. When the orientation is random, $w = 1/8\pi^2$.

REFERENCES

Birring, A. S., Alcazer, D. G., Hanley, J. J. and Gehl, S. (1989) Detection of creep damage by ultrasonics. In *Review of Progress in Quantitative Nondestructive Evaluation*, 8B. (eds D. O. Thompson and D. E. Chimenti). Plenum Press, New York, pp. 1833–1840.

Dunn, M. L. and Ledbetter, H. M. (1996) Estimation of the orientation distribution of short-fiber composites using ultrasonic velocities. *Journal of the Acoustical Society of America* **99,** 283–291.

Hirao, M., Aoki, K. and Fukuoka, H. (1987) Texture of polycrystalline metals characterized by ultrasonic velocity measurements. *Journal of the Acoustical Society of America* **81,** 1434–1440.

Hirao, M., Morishita, T. and Fukuoka, H. (1990) Ultrasonic velocity change with creep damage in copper. *Metallic Transactions* **21A,** 1725–1732.

Ledbetter, H. M., Datta, S. K. and Kriz, R. D. (1984) Elastic constants of an anisotropic, nonhomogeneous particle-reinforced composite. *Acta Metallica* **32,** 2225–2231.

Ledbetter, H. M. and Datta, S. K. (1986) Effective wave speeds in an SiC-particle-reinforced Al composite. *Journal of the Acoustical Society of America* **79,** 239–248.

Ledbetter, H. M., Fields, R. J. and Datta, S. K. (1987) Creep cavities in copper: an ultrasonic velocity and composite-modeling study. *Acta Metallica* **35,** 2393–2398.

Mori, T. and Tanaka, K. (1973) Average stress in matrix and average elastic energy of materials with misfitting inclusions. *Acta Metallica* **21,** 571–574.

Powell, M. J. D. (1964) An efficient method for finding the minimum of a function of several variables without calculating derivatives. *Computer Journal* **7,** 155–162.

Ratclife, R. T. (1965) The measurement of small density changes in solids. *British Journal of Applied Physics* **16,** 1193–1196.

Roe, R.-J. (1965) Description of crystallite orientation in polycrystalline materials. III. general solution to pole figure inversion. *Journal of Applied Physics* **36,** 2024–2031.

Sayers, C. M. (1982) Ultrasonic velocities in anisotropic polycrystalline aggregates. *Journal of Physics D* **15,** 2157–2167.

Sayers, C. M. (1990) Inversion of ultrasonic wave velocity measurements to obtain the microcrack orientation distribution function in rocks. *Engineering Fracture Mechanics* **35,** 743–749.

Sayers, C. M. (1992) Elastic anisotropy of short-fibre reinforced composites. *International Journal of Solids and Structures* **29,** 2933–2944.

Tandon, G. P. and Weng, G. J. (1984) The effect of aspect ratio of inclusions on the elastic properties of unidirectionally aligned composites. *Polymer Composites* **5,** 327–333.

Weng, G. J. (1984) Some elastic properties of reinforced solids, with special reference to isotropic ones containing spherical inclusions. *International Journal of Engineering Science* **22,** 845–856.

Willems, H., Bendick, W. and Weber, H. (1987) Nondestructive evaluation of creep damage in service exposed 14 MoV 63 steel. In *Nondestructive Characterization of Materials II*, (eds J. F. Bussière, J.-P. Monchalin, C. O. Ruud and R. E. Green, Jr.). Plenum Press, New York, pp. 451–459.

Willems, H. (1987) Investigation on creep damage in alloy 800H using ultrasonic velocity measurements. In *Nondestructive Characterization of Materials II*, (eds J. F. Bussière, J.-P. Monchalin, C. O. Ruud and R. E. Green, Jr.). Plenum Press, New York, pp. 471–479.

Zhao, Y. H., Tandon, G. P. and Weng, G. J. (1989) Elastic moduli for a class of porous materials. *Acta Mechanica* **76,** 105–130.